Computers in Biology and Medicine 111 (2019) 103337

Contents lists available at ScienceDirect

Computers in Biology and Medicine

journal homepage: www.elsevier.com/locate/compbiomed

Simulation of biopsy bevel-tipped needle insertion into soft-gel

Mohamed Gouse Jushiddi[a,b,c], John J.E. Mulvihill[b,c,**], Drahomir Chovan[a], Aladin Mani[a], Camelia Shanahan[a,b], Christophe Silien[b,c], Syed Ansar Md Tofail[a,c], Peter Tiernan[b,c,*]

[a] Modeling, Simulation and Innovative Characterisation (MOSAIC), Bernal Institute and Department of Physics, University of Limerick, Limerick, Ireland
[b] School of Engineering, Faculty of Science and Engineering, University of Limerick, Limerick, Ireland
[c] Bernal Institute, University of Limerick, Limerick, Ireland

ARTICLE INFO

Keywords:
Needle insertion
Bevel-tipped
Biopsy needle
Finite element analysis
Coupled eulerian Lagrangian method
Needle deflection

ABSTRACT

Planning and practice of surgical procedures can be improved through the use of modelling. This study provides an insight into the biopsy needle (i.e. hollow cannula) and needle-tissue interactions using a modelling approach, thus enabling the optimization of needle-tip designs not only for training but also for the planning of surgical procedures. Simulations of needle insertion into agar gel were performed using a Coupled Eulerian-Lagrangian (CEL) based finite element (FE) analysis, adapted for large deformation and tissue fracture. The experimental work covers needle insertion into 3% agar gel using a needle with a beveled tip of various angles, to assess the validity of the simulation. The simulated needle deflection and insertion force for two needles (i.e. Needle 1 with 18° bevel angle and Needle 2 with 27° bevel angle) were compared with corresponding experimental results. The contact stress (i.e. contact pressure) on the needles from the agar gel during the insertion of the needles were also studied. Observations indicate that varying the needle bevel angle from 27° to 18° results in a decrease of the peak force (i.e. puncture force) and an increase in needle deflection. Quantitatively, the percentage errors between the experimental data and the FE model for the total insertion force along the z-direction (i.e. Z Force) for Needle 1 and 2 were 4% and 4.8% ($p > 0.05$), respectively. Similarly, needle deflection percentage errors along the *x-z* plane were 5.7% and 10% respectively. Therefore, the forces and needle deflection values predicted by the simulation are a close approximation of the experimental model, validating the Coupled Eulerian-Lagrangian based FE model. Thus, providing an experimentally validated model for biopsy and cytology needle design *in silico* that has the potential to replace the current build and break approach of needle design used by manufacturers.

1. Introduction

Needles are ubiquitous medical tools widely used in minimally invasive surgical and percutaneous procedures such as injection, regional anesthesia, blood sampling, biopsy and brachytherapy [1–3]. They come in a wide variety of needle tip configurations, such as bevel-tip, lancet tip, back-bevel tip, trocar, franseen, and conical, etc. Depending on the medical procedure in which they are used [1–4]. The minimally invasive surgical procedure is a common method that involves the insertion of a hollow needle (i.e. cannula) to a target inside the body for either tissue sample removal (i.e. biopsy) or drug delivery (i.e. brachytherapy). During this procedure, the accuracy of needle placement is of utmost importance, as tip misplacement in drug delivery or biopsy of an unintended tissue region may reduce the effectiveness and conclusiveness of the diagnosis and treatment, respectively. The inaccuracy of needle placement or needle deviation from its intended path is due to several factors such as tissue deformation (e.g. inhomogeneity and anisotropy), physiological processes (e.g. fluid flow and respiration) and anatomical obstructions [5–7]. However, the success of the minimally invasive surgical procedure also involves other factors such as needle tip force and friction during insertion causing additional tissue deformation and leading to the deflection of the needle from the target [8]. These inaccuracies and target placement errors can be reduced by using a robotic system for needle insertion that predicts needle deflection and also steers the needle towards the target [8–14]. Such use of a robotic system requires knowledge of needle-tissue interaction

* Corresponding author. School of Engineering, Faculty of Science and Engineering, University of Limerick, Limerick, Ireland.
** Corresponding author. School of Engineering, Bernal Institute and the Health Research Institute, University of Limerick, Limerick, Ireland.
E-mail addresses: Mohamed.Jushiddi@ul.ie (M.G. Jushiddi), John.Mulvihill@ul.ie (J.J.E. Mulvihill), Drahomir.Chovan@ul.ie (D. Chovan), Aladin.Mani@ul.ie (A. Mani), Camelia.Shanahan@ul.ie (C. Shanahan), Christophe.Silien@ul.ie (C. Silien), Tofail.Syed@ul.ie (S.A. Md Tofail), Peter.Tiernan@ul.ie (P. Tiernan).

https://doi.org/10.1016/j.compbiomed.2019.103337
Received 11 March 2019; Received in revised form 13 June 2019; Accepted 18 June 2019
0010-4825/ © 2019 Elsevier Ltd. All rights reserved.

dynamics that can be gained through experimentation or simulation-based methods such as finite element (FE) analysis [2,3,5,15–22].

In recent years, substantial research has been conducted on needle-tissue interaction through experimentation of needle insertion into soft gel [16–19]. These studies investigate the effect of selected parameters such as diameter, bevel angle, needle insertion speed, needle tip geometry and gel elasticity, which influence the interactions between the needle and soft tissue. In an experimental based study by Jiang et al. [16], it was shown during needle insertion that varying parameters such as diameter, bevel angle, insertion speed and tip shape, result in alterations of the needle forces and gel rupture. van Gerwen et al. [17] carried out a review of the experimental studies of needle force interactions with tissue and found that typical peak forces are on the order of 0.1–10 N. The study also highlighted that blunt-tipped needles produce higher peak axial force than the conical, diamond and bevel needles, despite smaller diameters.

Extensive research has been carried out in the development of the surgical needle-tissue interaction model to simulate real-time behaviour using finite element (FE) method [5,6,20,21]. FE analysis of the needle-tissue insertion mechanism in surgical simulation needs to take several factors into account such as material mechanical behaviour (tissue/soft gel), material and geometry non-linearity (large deformation), material rupture (puncture) and boundary conditions (contacts) [5–7]. Misra et al. [19] presented a comprehensive review of the literature related to the modelling of needle-tissue interaction using the FE method and its application in modelling simulations for the invasive and non-invasive surgical method in the medical field. FE analysis with an element deletion method can be used to simulate puncture or rupture at the needle tip [5,20]. However, this modelling method requires small elements in the region of needle-tissue interaction, which results in high computational time. This method may also result in unreliable results due to deletion of elements in the vicinity of the needle when large deformation occurs (i.e. needle penetration). Subsequently, Oldfield et al. [20] proposed an FE method with a cohesive zone element model or crack propagation using a cohesive element to simulate tissue rupture and needle-tissue interaction. In this technique, the cutting and subsequent needle penetration path need to be defined prior to needle insertion, and the initiation of crack needs to be defined with the crack (i.e. notch) on the surface of the bulk material. The drawback of this method is that the needle path is not known prior to insertion and may lead to a distribution of cohesive elements over a region with very fine elements. This distribution of cohesive elements can lead to higher computation time as they make it difficult to define the crack propagation path. In the literature [2,18,20], most of the linear elasticity models are based on indentation and element deletion or element splitting (i.e. adaptive re-meshing technique).

Recently, another FE method was proposed by Yamaguchi et al. [21] using Arbitrary Lagrangian Eulerian (ALE) based technique. This method is used in the fluid based analysis, that involves large deformation and fracture in continuum models. The advantages of this method include; its ability to resolve arbitrary enclosing boundaries; to have changeable zoning for obtaining an optimum resolution, with improved accuracy in a problem where fully Lagrangian calculations are not possible; to function with time steps much larger than possible with explicit methods [23]. The study showed that the ALE based FE method enables dynamic analysis of needle insertion and can be used to study needle-interaction forces, needle deflection and needle tip geometries in soft phantom tissue environment. Phantoms are tissue mimicking materials that are commonly used to investigate needle-tissue interaction and for the training of clinicians in image-guided needle interventions [24]. In general, the use of biological tissue is not always a feasible option, due to practical and ethical issues. As the use of biological tissue is not always a feasible option due to practical and ethical issues; gels can provide an alternative. Gels can exhibit viscous, non-linear elastic behaviour that mimics biological tissue and are quite complex [16]. In general, gels are more durable and can be customised to the needs of specific research activities or training [25]. Coupled Eulerian-Lagrangian (CEL) method in ABAQUS is a similar technique which can simulate large deformation and fracture problems using fluid-structure analysis [25].

This study aims to develop a three-dimensional (3D) FE model to simulate needle-tissue interaction of biopsy needle (i.e. cannula) during manual surgical insertion in soft tissues using commercially available FE software Abaqus. The application of the study is to develop an *in silico* model to understand forces and factors that can influence a robust needle design for biopsy applications. As a first approximation, the present study focuses on developing an FE analysis linear elastic model that predicts the needle interaction dynamics with gel as a substitute for the soft biological tissue. In the analysis, a Coupled Eulerian-Lagrangian (CEL) based FE method was used to perform dynamic analysis of needle insertion into a soft gel. van Gerwen et al. [17] have reviewed the literature on solid needle insertion models which use the tip and shaft forces and needle deflection as defining parameters. These models must be modified to account for needle geometry such as bevel type and bevel angles in the hollow needles as well as the contact area between the needle cutting edge and phantom tissue.

To the best of the authors' knowledge, this study investigates for the first time the modelling of a 3D hollow needle insertion into gel using CEL based FE method and presents a comparison of simulation results with experimental data acquired through the use of a high speed camera. The model also predicts and could help us to understand, how a hollow needle, particularly the cutting edge and needle tip design, affect needle forces and deflection during the needle insertion process. Thus, providing an experimentally validated model for biopsy and cytology needle design *in silico* that has the potential to replace the current build and break approach of needle design used by manufacturers. This model can form an indispensable tool to study needle design for more effective hollow needle tip geometries for surgical procedures. The model can also help with planning, training, and practice of surgical procedures in handheld or robot-assisted surgery.

2. Material and method

2.1. Specimen preparation and test conditions

Agar gel is commonly used for the cell culture of cartilage and soft tissue. It has also been used as a phantom material for imaging techniques due to its material properties [21,26]. Gel with Agar (Agar-05038, Sigma-Aldrich, USA) concentration (weight/volume, w/v) of 3% was prepared by dissolving powdered agar in distilled water. The solution was sealed and heated for 15 min at 90–95 °C and magnetically stirred until the agar powder was completely dissolved. Finally, the solution was left in the beaker to cool down to 60 °C before it was poured into a cylindrical mould and left overnight at room temperature to cure. To ensure consistent test conditions across the experiments, transparent acrylic Petri dishes (cell culture dish), 85 mm in diameter and 15 mm in height were used as a mould and covered with a lid to maintain humidity and to prevent moisture loss. Storage time before testing was kept constant throughout the study, within allowable limits (18 h and 30 ± 5 min), to ensure comparable gel properties and reproducible data. The preparation of all specimens and the testing were performed under controlled laboratory conditions; 20 °C with 50% relative humidity. Agar gel samples were punched out in a cylindrical shape, nominally 50 mm in diameter and 10 mm in height. Ten cylindrical test samples were prepared for the test (compression test: Ø50 × 10 mm cross-head speed: 2.5 mm/s).

2.2. Characterization of mechanical properties of agar gel

A uniaxial compression test on agar samples as shown in Fig. 1 (a) was performed to obtain mechanical properties. These were then used as inputs in FE analysis to create a material model to simulate gel.

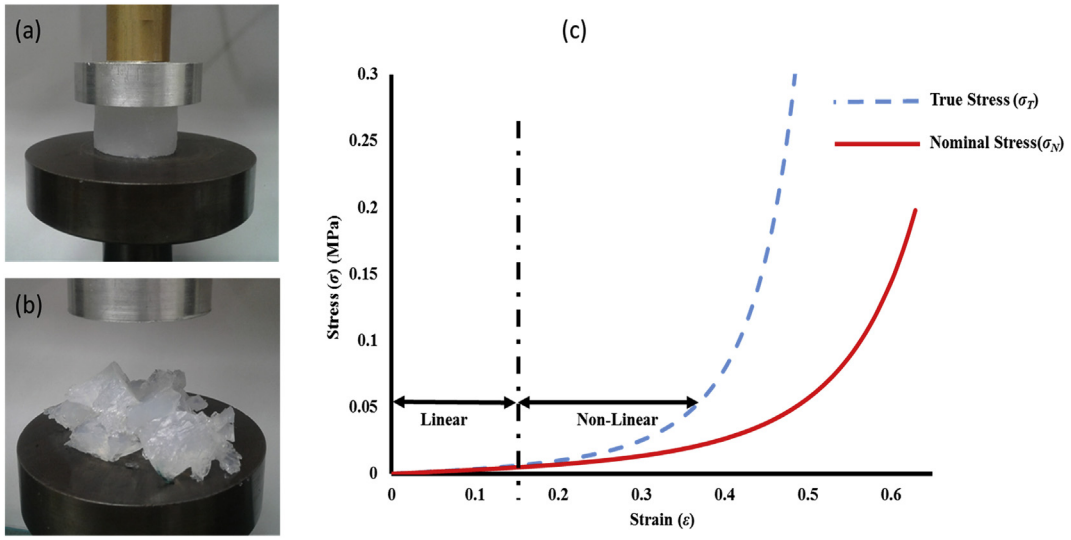

Fig. 1. Compression test of Agar Gel at a compression speed of 2.5 mm/s: (a) Cylindrical gel sample between loading plates (b) Gel sample completely damaged after compression test and (c) Compression stress-strain response. (i) Red continuous line indicates the nominal stress-strain curve and (ii) Blue dotted line indicates the true stress-strain curve. (i.e. 0–15% strain is considered to be linear region and 15–40% strain – non-linear region).

During the experiment, loading in compression mode was conducted on the cylindrical gel sample positioned between the loading plates of a Tinius testing machine with a 1000 N load cell (Tinius Olsen, H25KS Tinius Olsen Ltd. - United Kingdom). To achieve frictionless contact between the loading plate and the test sample and to ensure pure compression, paraffin oil was applied on the outer surface of the gel samples. The test was repeated for ten samples at a compression speed of 2.5 mm/s and the resulting force and displacement were recorded. Subsequently, this information was used to calculate true stress (σ_t) and true strain (ε_t) from the nominal stress-strain curve [5]. (See Supplementary file for more information).

In general, soft biologicaltissues are inhomogeneous and exhibit non-linear, anisotropic and viscoelastic behaviour which makes them more complex to model. As a first approximation, this study focuses on linear elastic large deformation dynamic model that predicts needle-interaction forces in three-dimensions. Fig. 1c shows the compression stress-strain curve which is close to linear up to strains of 10–15%. The relationship was non-linear for strains greater than 15%, due to a combination of material inhomogeneity and viscoelasticity [27]. The region after the strain of 15% compression was neglected as most of the probing and insertion experiments operate with strains below 15% [17,18]. From the initial slope of the curve (i.e. linear region) as shown in Fig. 1c, Elastic Modulus (E) was approximately found to be 0.0279 MPa. As the soft gel is considered to be nearly incompressible, the Poisson's ratio (ν) was set as 0.49 (i.e. 0.47 to 0.5 is commonly used) [18–21]. In linear elastic modelling, $\boldsymbol{E}$ and ν are the two material parameters used to define the soft tissue properties [18]. The FE simulation was performed using the parameters presented in Table 1.

2.3. Needle insertion experiment

To validate the needle insertion, an experimental procedure was developed to measure the needle insertion forces and deflection with a uniaxial insertion device. In the experiments, the needle was inserted into the agar gel at a constant velocity of 2.5 mm/s to a penetration depth of 50 mm with a uniaxial tensile tester (insertion device) as shown in Fig. 2. A similar test is performed in industry with custom made insertion devices to measure needle deflection and reaction forces [20,21]. In this test, the penetration forces at the needle tip and friction forces at the needle shaft are measured using a 100 N load cell (S-Type, Tinius Olsen DBBMTOL-100 N) placed above the needle holder (collet-chuck fixture). The size of the needle was Ø 0.9 mm × 125 mm based on a 20G surgical needle (stubs wire-gauge standard, ISO 9626) while the agar block dimensions were 100 × 40 × 150 $(mm)^3$. The angles of the bevel needle tip were 18° and 27° for needle 1 and 2 respectively, as shown in Fig. 3. Several studies have experimentally evaluated the effect of the bevel angle on the cutting forces of needles [4,16,28,29]. Jason et al. have shown that the cutting force shows a linear dependence for lower bevel angles (> 20°) and plateaus for higher bevel angles [30]. Moreover, the chosen bevel angles fall in the range of prevalently used bevel needles in surgical applications [16,29,30]. Elastic modulus (E) and Poisson's ratio (ν) of the 20G bevel tip steel needles (Cook Medical, Ireland, custom made) used were 200 GPa and 0.29 , respectively. To estimate the needle deflection, a rectangular Perspex box mould (100 × 40 × 150 mm^3) was prepared with one open end and an acetate graph sheet glued to the front of the Perspex box (Fig. 2b). The box was then filled with gel. The deflection of the needle was captured on videos and photos taken from the lateral side with a digital single-lens reflex camera (Nikon D5300, Nikon Corp, Japan) during insertion. Two 20 G one-plane symmetric needles with bevel angles of 18° and 27° were each inserted into agar gel ten times, leading to a total of 20 trials (Fig. 3). The insertion force at the final depth of the needle at 50 mm was recorded along with the initial puncture force to validate the needle insertion simulation model as shown in Fig. 4. In each case, the force along the z-direction (Z force) against the needle insertion depth was measured.

Supplementary video related to this article can be found at https://doi.org/10.1016/j.compbiomed.2019.103337.

Table 1
Linear model parameters (3% w/w agar gel) used in the FE model.

Parameters	Elastic Modulus (E) [MPa]	Poisson's ratio (ν)	Density (ρ) [g/cm^3]
Values	0.0279	0.49	1.172

2.4. CEL-based finite element analysis

A dynamic explicit CEL based linear FE model was developed using ABAQUS as shown in Fig. 4 [31]. The 3D FE model consists of the needle and the agar gel block. The needle is constrained along the **x** and **y**-axis at the proximal rigid part (red part of Fig. 4a) and a displacement of 50 mm was applied along the **z**-axis to this rigid part of the needle.

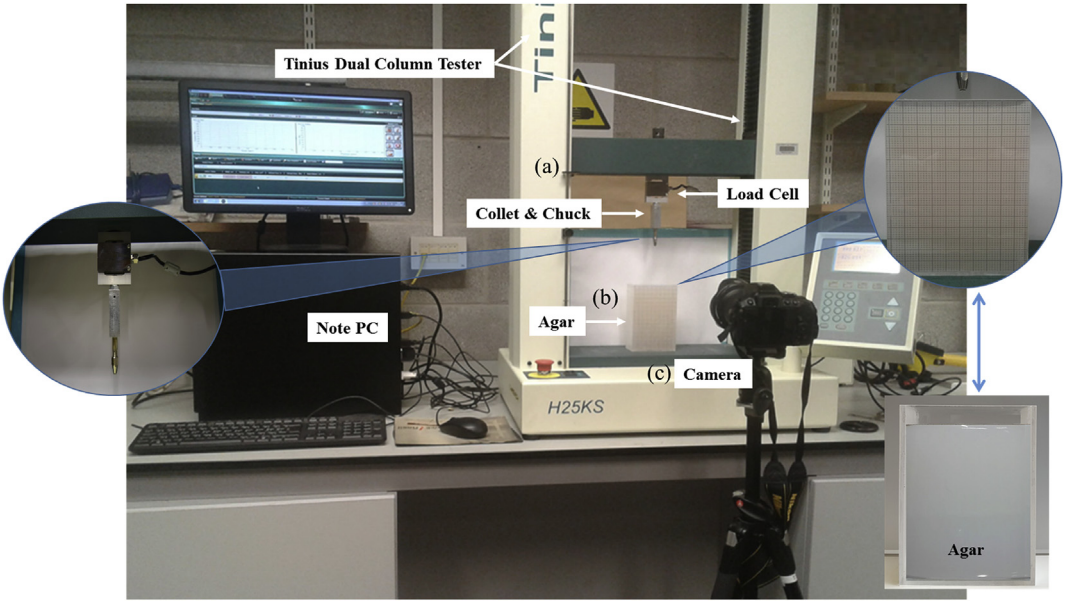

Fig. 2. Uniaxial tensile setup. (a) Tinius Dual Column tester fitted with a 100 N load cell and custom made collet-chuck fixture to hold a needle, (b) Agar mould inside the perspex glass encasing, and (c) Digital single-lens reflex camera to capture deflection of the needle.

The friction coefficient relates to the tangential interaction between the needle and the agar gel [21]. A friction coefficient of 0.02 was iteratively found to best fit experimental data. This is an order of magnitude lower than the friction coefficient of agar gel determined experimentally using indirect methods [32], which makes it difficult to relate the friction coefficient used in the simulation to a patient-specific scenario. As for insertion, we have used a speed of 2.5 mm/s both simulation and experiment. Switching to a higher insertion speed (4 mm/s) had little impact on the insertion force, which is in line with what has been observed in the case of solid needle insertion experiments at different speeds [16]. The geometries for needles and agar gel were adopted corresponding to the experimental setup (Fig. 2) and the angles of the bevel needle tip (Fig. 3). The material properties of agar gel were determined by the experiment and used in the creation of the agar gel material model (Table 1). The needle geometry was discretized using linear solid hexahedral elements with reduced integration and hourglass control, while the agar gel meshed with linear Eulerian brick, reduced integration, hourglass control (Fig. 4b and c) with 340,800 elements in total. The smallest element size adopted was 0.1 mm in all models. Finite element simulation for needle 1 was performed with different mesh densities between 0.1 and 0.5 to assess the effect of mesh density on simulation results. A mesh density of 0.5 mm has yielded a good agreement with experiment. Therefore, it was selected as an optimal mesh density. This mesh density when employed for needle 2 resulted in equally accurate prediction, confirming that the chosen mesh density is optimal. The total simulation time for modeling was set at 20 s for the 50 mm insertion, which matched the experiments.

2.5. Needle forces and contact stress

A typical needle insertion process involves three basic phases of interaction as shown in Fig. 5,which are distinguished as follows:

(a) Deformation (Phase 1): The first phase (see Fig. 5) starts when the needle tip comes in contact with the tissue/gel surface or tissue/gel boundary and ends when the tissue/gel surface or boundary is ruptured and the insertion force reaches a peak value known as peak force (F_N). The actual event of rupturing of the boundary is referred to as “puncture”.
(b) Tip Insertion (Phase 2): The second phase commences when the

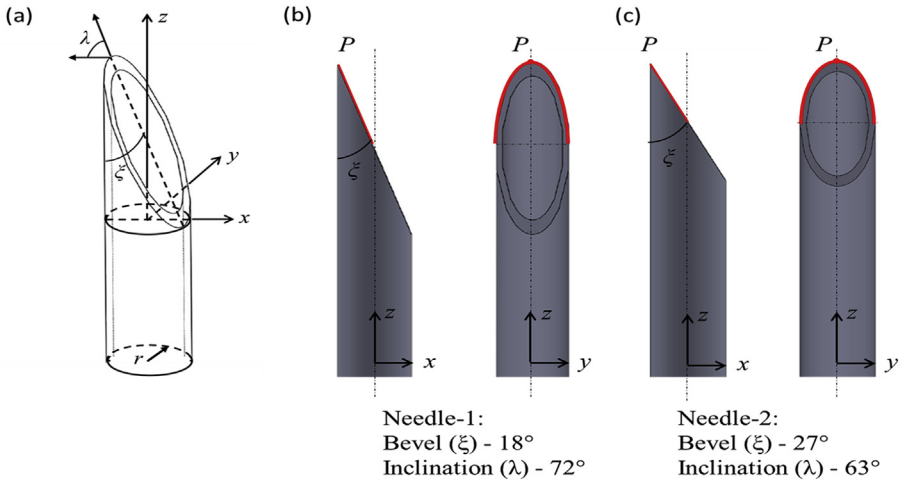

Fig. 3. Bevel tipped needle with various bevel angles. P indicates the point of contact and the red line indicates the cutting edge. (a) Illustration of the needle tip with bevel angle (ξ) and inclination angle (λ), (b) Needle 1 with 18° bevel angle, (c) Needle 2 with 27° bevel angle.

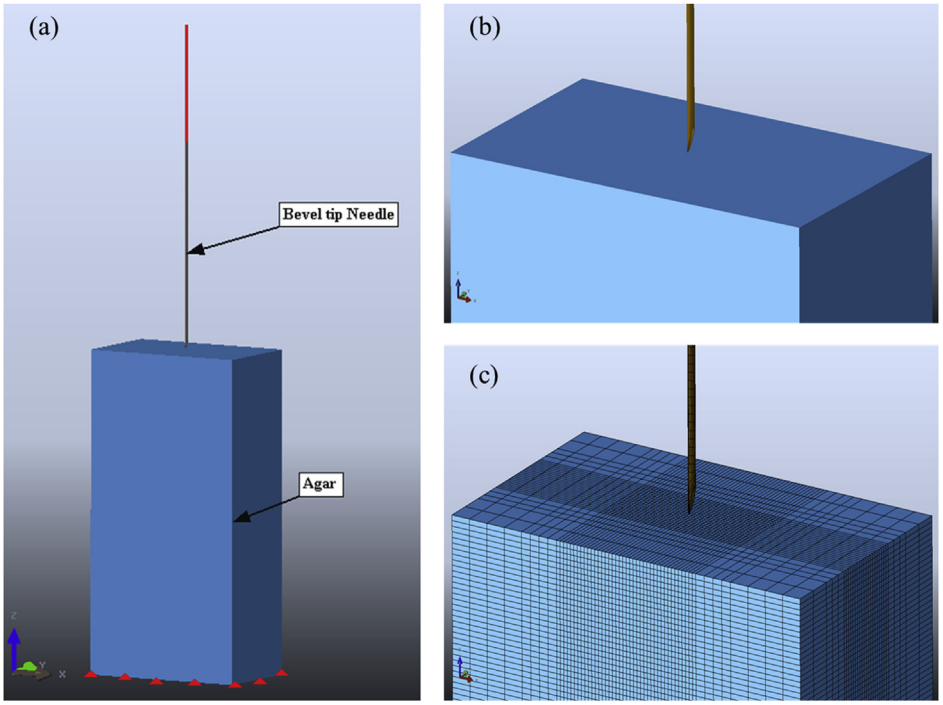

Fig. 4. Finite element model for needle insertion analysis: (a) Solid model with a bevel needle fixed at a rigid part (i.e. red part) and gel constraint at the bottom part. (b) Close up section at the needle tip and agar gel, and (c) Meshed model with the solid hexahedral element.

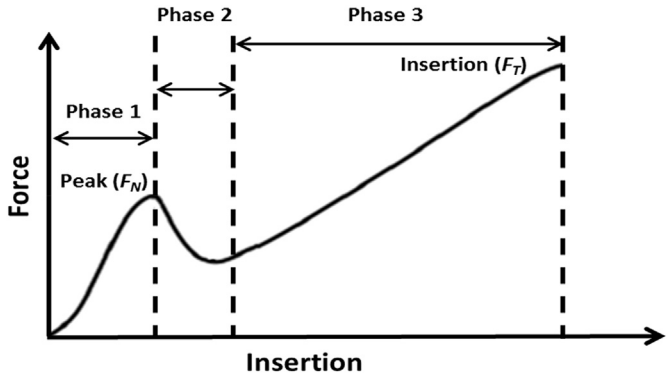

Fig. 5. A typical needle insertion process (i.e. Phase 1 – Deformation ends with Peak force (F_N); Phase 2 – Tip insertion; and Phase 3 – Tip and shaft insertion ends with total Insertion force (F_T).

tissue/gel surface or boundary is ruptured and it ends when the tissue or gel (i.e. phantom soft tissue) slides over from the tip onto the shaft.

(c) Tip and Shaft Insertion (Phase 3): The third phase starts just after the tip insertion, which is a transition from the tip to the shaft and ends when the needle encounters a new tissue boundary (internal), or it is stopped. During this insertion phase, the needle tip is subjected to cutting force and needle shaft to a varying frictional force due to the increase in the contact area between the shaft and tissue as the needle is advanced.

The contact stress or radial stress on the needle-tissue interaction can be divided into two components: normal stress (i.e. axial) and shear stress (i.e. frictional). However, these stresses result from the contact pressure (CP) between the needle and tissue/gel interaction during the needle insertion process. This contact pressure induces the normal force and tangential frictional force on the needle shaft from tissue/gel interaction during needle insertion. Assuming constant frictional coefficient and increasing contact area along the inserted needle length, results in frictional stress which is in turn related to the radial stress.

2.6. Statistical analysis

The experimental data are represented as a mean ± standard error about the mean; for deflection, peak force and insertion force. The normality of these datasets was examined using the D'Agostino and Pearson test, all of which were found to be normally distributed. Significant differences were identified between experimental groups of continuous variables using Student t-test for the normally distributed data. For comparison of experimental with simulation data for both needles, a two-way analysis of variance (ANOVA) test was used to compare the mean values of the different groups. A p-value (alpha value) < 0.05 was considered statistically significant for all tests.

3. Results

3.1. Needle deflection

Comparison of needle deflection for the two bevel tips between the experimental and simulation results is shown in Fig. 6. The difference in mean deflection for the 18° and 27° bevel angle needles, compared to experiments, were 0.25 mm and 0.4 mm, respectively. The lateral deflection of the 18° bevel tip needle is captured from the image at approx.50 mm as shown in Fig. 7. The photos of needle insertion in agar gel at 10, 20, 30, 40, and 50 mm during needle the insertion experiment are shown in appendix A (Fig. A1).

3.2. Needle forces

Comparison of needle force insertion curve between the experimental and simulation results for 18° bevel tipped needle (Needle 1) is shown in Fig. 8. It is evident from the measured forces, that the varying frictional force leads to an increase of insertion force (i.e. cutting and friction) as shown in typical needle insertion process (see Fig. 5). Hence, the total insertion force (F_T) comprises of puncture force (i.e. cutting) and friction force (i.e. penetration). For the oscillations (i.e.

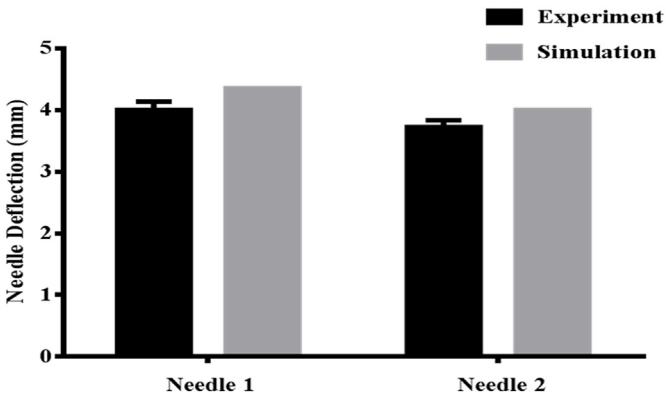

Fig. 6. Comparison of needle deflection at 50 mm in-depth between result of experiments and simulation for needle 1 (18 deg) and 2 (27deg).

noise) in the simulated reaction force curve (i.e. Z Force) from FE analysis, the dataset was smoothened and normalized using data analysis software (Origin Pro8). The measured initial peak force (i.e. maximum, mean and minimum) of all 10 repeated experiments for Needle 1 and Needle 2, along with the simulated peak force from the FE analysis are plotted in Fig. 9. Fig. 9 also presents the result of measured total insertion force for both the Needle 1 and Needle 2 along with the simulated total insertion force from the FE analysis, respectively. The percentage of error between the experimentally measured (mean) and simulated peak force (F_N) for needles 1 and 2 are 15.2% and 15.6% (Table 2). However, the percentage of error between the measured and simulated total insertion force (F_T) for both the needles is 4% and 4.2% respectively.

3.3. Needle contact stress

Comparison of needle contact stress (see section 2.5) for needles 1 and 2, based on simulations, is shown in Fig. 10. The contact stress distribution for Needle 1 along the cross-sectional surface in the *x-z* plane for initial puncture and for each 10 mm insertion, is shown in Fig. 11. Subsequently, after a puncture, the maximum contact stress appeared to be moving along the shaft from needle tip throughout the needle insertion for both of the models. The initial peak contact stresses at the event of a puncture during needle insertion for Needle 1 and Needle 2 were 125 MPa and 110 MPa, respectively.

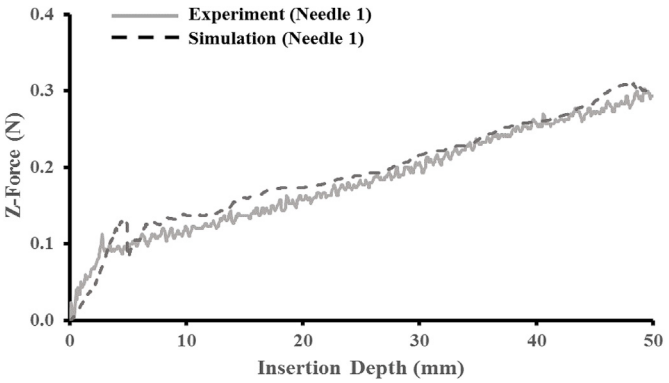

Fig. 8. Comparison of reaction force (Z-Force) between the result of one representative experiment and simulation for needle 1(18deg).

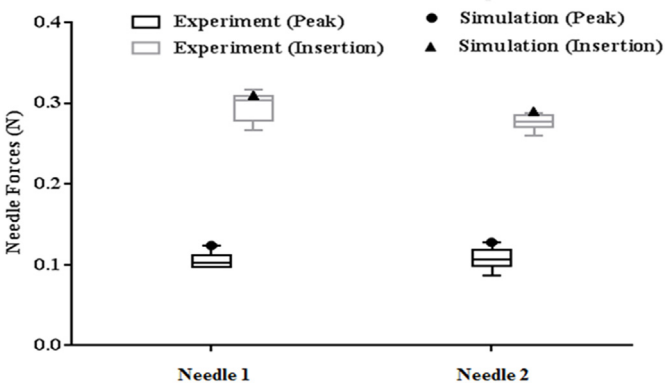

Fig. 9. Comparison between all representative experimental results (mean ± standard error) of needle insertion forces (i.e. peak and insertion force) and model predicted result.

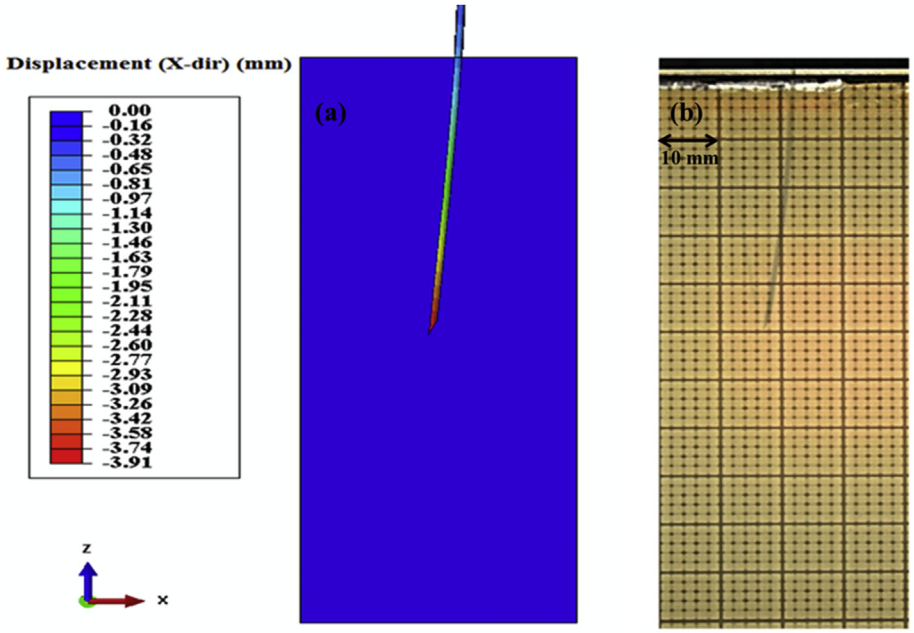

Fig. 7. Needle deflection at 50 mm in-depth: (a) Simulation result for needle 1 (18deg) (i.e. Deflection (D) = 3.91 + 0.45 outer diameter (O.D) of needle) and (b) Experimental result for needle 1 (18deg) (i.e. D = 2mm/dot).

Table 2
Comparison of needle insertion forces at 50 mm in-depth between results of experiments and simulation for Needle 1 and Needle 2.

Needles		Angle	Bevel Length (mm)	Initial Peak Insertion Force, F_N			Total Insertion Force, F_T		
				Measured (Mean) (N)	Simulated (N)	Error (%)	Measured (Mean) (N)	Simulated (N)	Error (%)
Needle 1		ξ = 18°	2.95	0.106	0.125	15.2	0.295	0.31	4.0
Needle 2	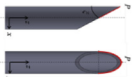	ξ = 27°	2.01	0.108	0.128	15.6	0.276	0.29	4.8

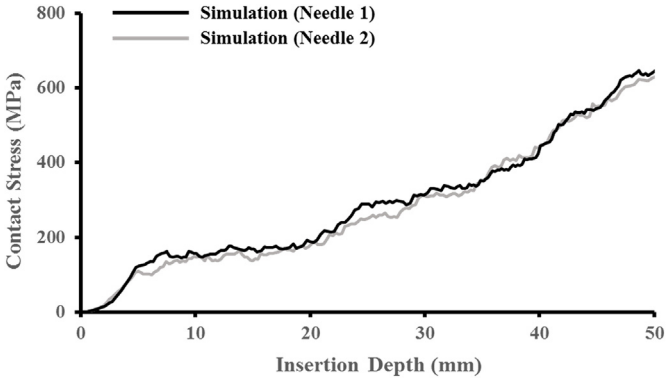

Fig. 10. Comparison between Needle 1 (18deg) and Needle 2 (27deg) contact stresses on the needle (Z-stress) from needle insertion simulation.

4. Discussion

In this study, a 3D FE analysis model was developed for hollow needle insertion into soft agar gel through CEL based FE method using dynamic fracture analysis. Applying a CEL method to structure analysis (i.e. FE analysis) makes it possible to do fluid-structure analysis with large deformation and fracture. The aim of this study was to create a numerical FE model to enable the better understanding of the needle-tissue interaction *in silico* and ultimately optimize the performance of hollow needle tip design to overcome the existing shortcomings of current hollow needle design. Moreover, the needle insertion experimental test setup model into soft gel was developed and quantitatively analyzed to evaluate and validate the simulation model. Experimental work has identified forces (due to puncture, cutting and friction) developed during needle insertion through phantom tissue (i.e. agar gel). While the study can provide useful insights into the distal force dynamics relevant to robot-assisted needle insertion (please see Adagolodjo et al. [22] for details), it does not address machine-driven needle insertion. The study rather involved investigations of interaction forces working at the needle tip and shaft.

In the literature [2,5,12,15,16,28], it is clear that the shape and size of the needle play a substantial role in determining the forces of needle insertion. In general, a needle with a smaller diameters leads to less insertion force but more needle bending [28]. Bevel tipped needles leads to more bending and higher peak force compared to the cone and triangular tipped needle [16]. Although, despite this drawback, bevel tip are prevalent because of maneuverability, allowing the clinician to rotate the needle to deliver therapy in a different direction and ease of manufacture. In most minimally invasive surgical procedures, such as biopsy or drug delivery, a needle cannula (hollow needle) is used for tissue removal or seed implantation. Needle insertion is typically a tissue cutting process and depends greatly on the cutting edge geometry [3]. In this study modelling of a 3D hollow needle insertion into the gel is carried out for the first time. Needle tip geometry was defined only by the bevel angle which does not directly reveal any specific information about the cutting edges (Fig. 3).

The study performed for assessing the needle-tissue interaction mechanism involved creating FE models and simulating needle insertion and interaction with a phantom tissue (i.e. soft gel). The frictional coefficient of 0.02 was set analytically as the contact condition between the needle and gel because it was found to be in good agreement between the experimental and simulation result. In addition to this, T.L. de Jong et al. carried out a research to study the phantom tissue (PVA) as a liver tissue mimicking material and found PVA 4 m% with 2FT (freeze-thaw) cycles is the only specimen comparable to ex vivo human

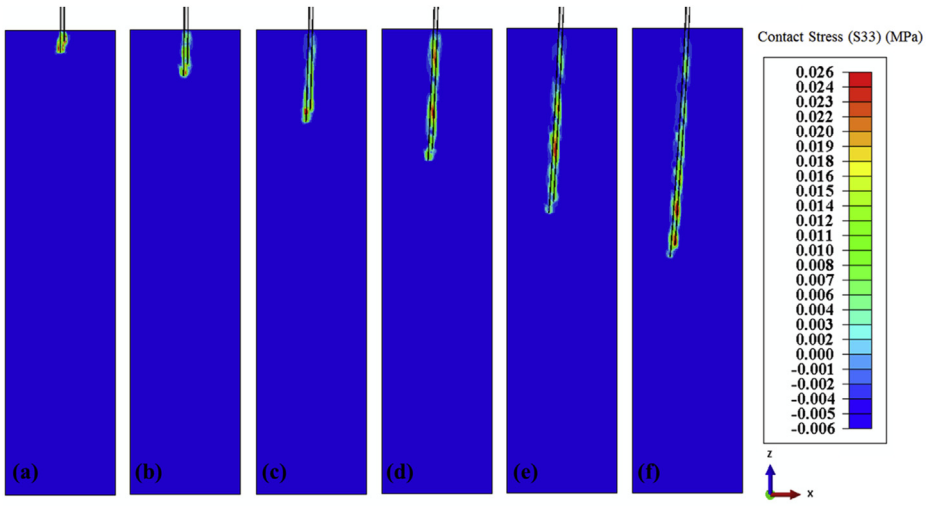

Fig. 11. Contact stress distributions around the needle for Needle 1 (18°) (MPa): (a) Puncture, (b) step10, (c) step20, (d) step30, (e) step40, and (f) step50.

liver. Moreover, it was found that the estimated median friction slope for the insertion into phantom tissue is in the range between 0.01 N/mm to 0.02 N/mm [24]. A mesh sensitivity study with varying mass density was also performed to investigate the effect of reducing global mesh size and increasing the step time (Δt) on the results of FE simulations. However, since large noise and oscillation in the curve occurred for simulated FE forces, for the larger density and mesh size, a finer mesh, and smaller Δt was recommended. In order to reduce the computational time and improve the accuracy of the forces, a trade-off between the larger density and optimum mesh size for the needle was considered. The simulation took approximately 70 h on a 12 core CPU (i.e. Intel dual-core Xeon 2.6 GHz, Memory: 16Gbyte), with mass scaling the density of needle to 10^5 times as large as the true value to finish analysis. Accordingly, Kataoka et al. proposed a needle insertion simulation model using Eulerian hydrocode FE method and highlighted the influence of density scaling on the simulated force has very little to no significant effect [25]. With regards to the computational time, as a solution for this issue, the general purpose graphics processing unit (GPGPU) has been developed which has accelerated the use of various commercial software in recent years [31]. In other words, with the application of GPGPU in the dynamic analysis (i.e. explicit analysis), the real-time computational based surgical simulation will appear soon.

This study presents both experimental and simulation results of needle-gel interactions. The experiments were conducted under constant velocity, constant needle diameter, needle tip shape, gel elasticity, and varying bevel angle. The uniaxial compression test was suitable for gel specimens because it is simple and eliminates the problem of premature failure arising from clamping as in tensile tests [5,26,27]. To define the elastic modulus of agar gel, the initial slope of true stress-strain (i.e. linear region) was considered. It was observed from previous studies that most of needle or probe insertion methods undergo high deformation which is followed by a rupture event causing sudden crack propagation inside the gel/tissue when operating within the range of 15%–20% strain [17,18,33]. To imitate the intraoperative handheld insertion process, or continuous robotic insertion, a constant velocity of 2.5 mm/s was selected for the needle insertion experiment. During the experimental process, the interaction between the needle and the agar gel was observed. The results from experimental curves were found to be in good agreement with the typical graph for needle insertion in soft tissue/gel as shown in Fig. 5.

The results from FE simulation were compared with those of experiment with agar gel, including force and deflection data. For needle deflection, the percentage error along the x-z plane for Needle 1 and Needle 2 are 5.7% and 10%, respectively (Fig. 6). Fig. 6 also demonstrates that a needle with a lower bevel angle tends to have more deflection compared to one with a higher bevel angle. Similar trends were observed when compared to a result obtained by Yamaguchi et al. [21]. Moreover, in clinical practice, there is no defined tolerance for the accuracy of needle insertion, and in general, insertions with limited needle misplacement or target placement errors result in more effective treatment [12]. These suggest that our experimental results are within the allowable range for clinical application such as pre-operative surgical planning. In addition, the variation of the bevel angle does not lead to a significant variation between simulation estimates and experimental results in needle deflection (Fig. 6 and 7) ($p > 0.05$).

Quantitatively, the percentage errors between the experimental data and the FE simulation for the total insertion force along the z-direction (i.e. Z Force) for Needle 1 and Needle 2 were 4% and 4.8%, respectively (Table 2). Fig. 8, clearly demonstrates that the total insertion force in the simulation follows those in the experiment until the needle tip and shaft portion of the needle are completely inside the agar gel. For the insertion force (Fig. 8), there was a peak force during needle puncture that is comparable to a result obtained by Okamura et al. [28]. It is evident from the results, that needles with lower bevel angle (i.e. Needle 1) tend to have less peak force but higher insertion force compared to higher bevel angle needle (see Table .2). A larger bevel angle (ξ) reduces inclination angle (λ), thereby creating a higher peak force during needle insertion as observed by Han et al. [34]. Moreover, the simulated reaction force from FE analysis and the measured insertion force, obtained from experiments, showed no significant difference for the total insertion force throughout the needle insertion depth, for both of the tested bevel needle tips (Table 2) ($p > 0.05$). It is evident from the simulation and experimental result that the increase of insertion force after a puncture is due to the influence of friction between the agar gel and the needle (Fig. 8). In the literature [2,16,18,20,21], the force at the needle tip was almost flat after the needle tip penetrated the surface, while the friction force proportionally increased. This trend was achieved in our result because the force at the needle tip and the friction on the needle shaft were measured separately. It was observed that the cutting force (F_C) was almost flat after the needle tip insertion into the surface (i.e. puncture), while the friction force (F_F) increased proportionally along with the needle insertion depth (see Appendix A, Fig. A3).

Finally, the contact stress (i.e. contact pressure) along the needle surface due to the stick-slip effect of friction on the needle shaft could be the key parameter in the study of needle-tissue interaction for different biological tissues and different material coating for needles. The results from the simulation may help to predict needle deflection, insertion force and contact stress distributions during needle insertion as an *in silico* pre-operative surgical planning tool for procedures that require accurate needle targeting e.g. biopsy and brachytherapy. These results suggest that the FE model can be used to simulate 3D gel fracture due to large deformation and tip-gel interaction forces and needle stresses. However, the FE model presented here predicts the forces and deflection of the needle based on a linear elastic material model. Within the limitation of FE based CEL technique in Abaqus, the FE model is limited to needle deformation or deflection and cannot predict deformation for the gel. For more clinical situations, it is proposed that the current setup is adopted to investigate the applicability of our approach to investigate needle-tissue interaction for porcine liver as a biological substitute for gel.

5. Conclusion

In this study, a three-dimensional finite element needle insertion model was developed using CEL based FEA method. This model can offer an alternative approach to the needle design process by enabling and understanding the complex needle-tissue interaction with the different needle tip designs and their behaviour through computer simulations. The validity of the model suggests that it could be used as a tool to study clinical applications such as pre-operative surgical planning. Our results help to understand and predict the needle deflection, needle forces, and contact stress distribution during needle insertion as pre-operative surgical planning *in silico*. This model can form an indispensable tool not only for needle tip design but also help us to understand the needle cutting process during needle insertion, thus assisting in optimizing the current needles. For more clinical situation, the plan is to extend the outcome of this study for biological application by incorporating CEL based FE analysis for different needle tip designs and soft biological tissue interaction.

We successfully implemented a model that is based on the well-known Abaqus platform and can be adopted in commercial biopsy needle design much quicker than more complex, time-consuming models. It must be noted that modelling and simulations are hypothesis based and limited to boundary conditions. Heterogeneity, motion, anatomical location and types of tissues or organs make the in vivo situation quite different from what we have experimentally tested in agar gel. This approach is in line with the current practice of testing commercial needles in simple soft gel phantoms for preliminary validation. Further complexities can be built on to address the in vivo scenario more closely and should be studied in the future.

Conflicts of interest

The authors have declared that no conflict of interests exists.

Acknowledgments

This publication has emanated from research supported in part by a research grant from Science Foundation Ireland and it is co-funded under the European Regional Development Fund under Grant Number 13/RC/2073. The authors would like to thank John Neilan, David Murray, Jim Butler, and Fionan Keady of Cook Medical for their in-kind contribution of materials and computational resources for performing experiments and simulations.

Appendix A

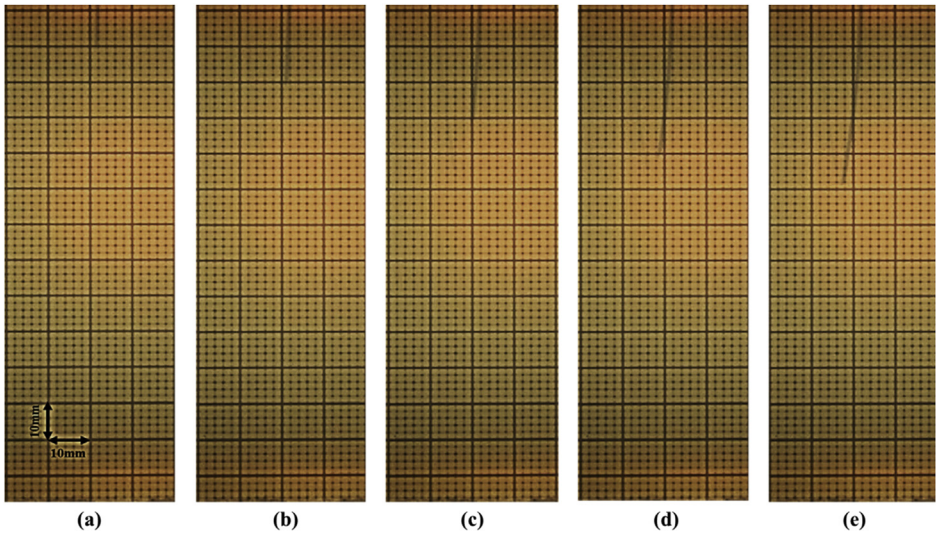

Fig. A1. Needle deflection during needle insertion experiment (18°) (mm): (a) step10, (b) step20, (c) step30, (d) step40, and (e) step50.

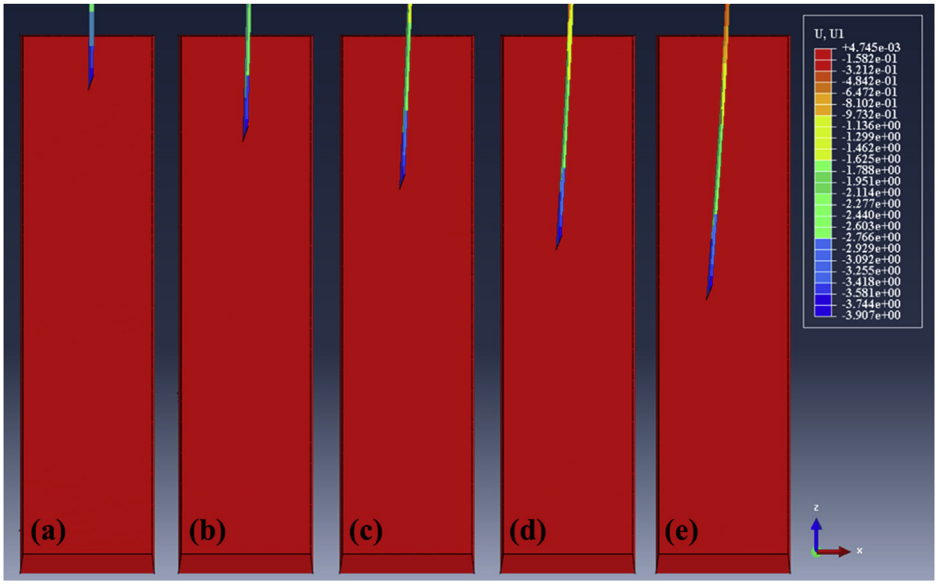

Fig. A2. Needle deflection during needle insertion simulation (18°) (mm): (a) step10, (b) step20, (c) step30, (d) step40, and (e) step50.

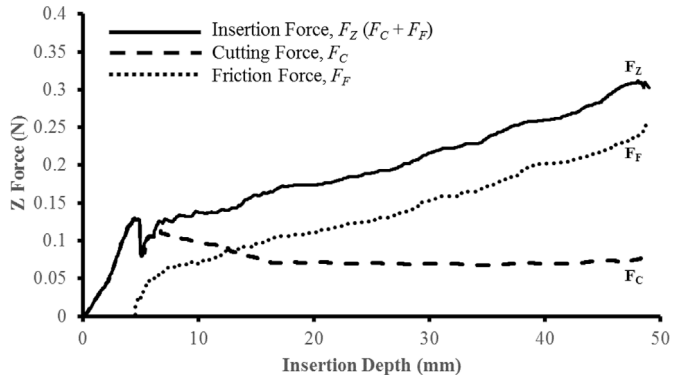

Fig. A3. Needle Reaction force (Z Force) (N1) during needle insertion simulation process.

Appendix B. Supplementary data

Supplementary data to this article can be found online at https://doi.org/10.1016/j.compbiomed.2019.103337.

References

[1] T.R. Kucklick, T.R. Kucklick (Ed.), Introduction to Needles and Cannulae, CRC Press Taylor and Francis Group, Boca Raton, FL, 200633487–2742.
[2] Y.R. van Veen, A. Jahya, S. Misra, Macroscopic and microscopic observations of needle insertion into gels, Proc. IME H J. Eng. Med. 226 (6) (2012) 441–449.
[3] P. Han, et al., Models of the cutting edge geometry of medical needles with applications to needle design, Int. J. Mech. Sci. 65 (1) (2012) 157–167.
[4] M.A. Towler, et al., Influence of cutting edge configuration on surgical needle penetration forces, J. Emerg. Med. 6 (6) (1988) 475–481.
[5] W. Assaad, et al., Finite-element modeling of a bevel-tipped needle interacting with gel, J. Mech. Med. Biol. 15 (05) (2015) 1550079.
[6] Jahya, A., F. van der Heijden, and S. Misra. Observations of three-dimensional needle deflection during insertion into soft tissue. in Biomedical Robotics and Biomechatronics (BioRob), 2012 4th IEEE RAS & EMBS International Conference on. 2012. IEEE.
[7] S.P. DiMaio, S.E. Salcudean, Interactive simulation of needle insertion models, IEEE Trans. Biomed. Eng. 52 (7) (2005) 1167–1179.
[8] K. Chinzei, et al., MR compatible surgical assist robot: system integration and preliminary feasibility study, International Conference on Medical Image Computing and Computer-Assisted Intervention, Springer, 2000.
[9] M. Abayazid, et al., Integrating deflection models and image feedback for real-time flexible needle steering, IEEE Trans. Robot. 29 (2) (2013) 542–553.
[10] S.P. DiMaio, S.E. Salcudean, Needle steering and motion planning in soft tissues, IEEE (Inst. Electr. Electron. Eng.) Trans. Biomed. Eng. 52 (6) (2005) 965–974.
[11] N. Abolhassani, R. Patel, M. Moallem, Control of soft tissue deformation during robotic needle insertion, Minim. Invasive Ther. Allied Technol. 15 (3) (2006) 165–176.
[12] N. Abolhassani, R. Patel, M. Moallem, Needle insertion into soft tissue: a survey, Med. Eng. Phys. 29 (4) (2007) 413–431.
[13] D. Glozman, M. Shoham, Image-guided robotic flexible needle steering, IEEE Trans. Robot. 23 (3) (2007) 459–467.
[14] S. Misra, et al., Mechanics of flexible needles robotically steered through soft tissue, Int. J. Robot. Res. 29 (13) (2010) 1640–1660.
[15] S. Misra, et al., Needle-tissue interaction forces for bevel-tip steerable needles, Biomedical Robotics and Biomechatronics, 2008. BioRob 2008. 2nd IEEE RAS & EMBS International Conference on, IEEE, 2008.
[16] S. Jiang, et al., Experimental study of needle–tissue interaction forces: effect of needle geometries, insertion methods and tissue characteristics, J. Biomech. 47 (13) (2014) 3344–3353.
[17] D.J. van Gerwen, J. Dankelman, J.J. van den Dobbelsteen, Needle–tissue interaction forces–A survey of experimental data, Med. Eng. Phys. 34 (6) (2012) 665–680.
[18] S.P. DiMaio, S.E. Salcudean, Needle insertion modeling and simulation, IEEE Trans. Robot. Autom. 19 (5) (2003) 864–875.
[19] S. Misra, K. Ramesh, A.M. Okamura, Modeling of Tool-Tissue Interactions for Computer-Based Surgical Simulation: A Literature, (2008).
[20] M. Oldfield, et al., Detailed finite element modelling of deep needle insertions into a soft tissue phantom using a cohesive approach, Comput. Methods Biomech. Biomed. Eng. 16 (5) (2013) 530–543.
[21] S. Yamaguchi, et al., Dynamic analysis of a needle insertion for soft materials: arbitrary Lagrangian–Eulerian-based three-dimensional finite element analysis, Comput. Biol. Med. 53 (2014) 42–47.
[22] Y. Adagolodjo, et al., Robotic insertion of flexible needle in deformable structures using inverse finite-element simulation, IEEE Trans. Robot. (2019) 1552–3098.
[23] J. Donea, S. Giuliani, J.-P. Halleux, An arbitrary Lagrangian-Eulerian finite element method for transient dynamic fluid-structure interactions, Comput. Methods Appl. Mech. Eng. 33 (1–3) (1982) 689–723.
[24] T.L. de Jong, et al., PVA matches human liver in needle-tissue interaction, J. Mech. Behav. Biomed. Mater. 69 (2017) 223–228, https://doi.org/10.1016/j.jmbbm.2017.01.014.
[25] H. Kataoka, et al., Simulations of needle insertion by using a eulerian hydrocode fem and the experimental validations, International Conference on Medical Image Computing and Computer-Assisted Intervention, Springer, 2008.
[26] E. Varoni, et al., Agarose gel as biomaterial or scaffold for implantation surgery: characterization, histological and histomorphometric study on soft tissue response, Connect. Tissue Res. 53 (6) (2012) 548–554.
[27] A. Forte, et al., Modelling and experimental characterisation of the rate dependent fracture properties of gelatine gels, Food Hydrocolloids 46 (2015) 180–190.
[28] A.M. Okamura, C. Simone, M.D. O'leary, Force modeling for needle insertion into soft tissue, IEEE Trans. Biomed. Eng. 51 (10) (2004) 1707–1716.
[29] S. Jiang, X. Wang, Mechanics-based interactive modeling for medical flexible needle insertion in consideration of nonlinear factors, J. Comput. Nonlinear Dyn. 11 (1) (2016) 011004.
[30] J.Z. Moore, et al., Hollow needle tissue insertion force model, CIRP Ann. - Manuf. Technol. 60 (1) (2011) 157–160.
[31] S. Abaqus, Dassault Systemes. Providence, RI, USA, (2011).
[32] F.A. Urrea, et al., Evaluation of the friction coefficient, the radial stress, and the damage work during needle insertions into agarose gels, J. Mech. Behav. Biomed. Mater. 56 (2016) 98–105.
[33] M. Mahvash, P.E. Dupont, Mechanics of dynamic needle insertion into a biological material, IEEE Trans. Biomed. Eng. 57 (4) (2010) 934–943, https://doi.org/10.1109/TBME.2009.2036856.
[34] P. Han, K. Pallav, K. Ehmann, Force Model for Needle-Tissue Interaction, (2012), pp. 51–58, https://doi.org/10.1115/MSEC2012-7257 54990.